

ChemComm

Accepted Manuscript



This is an *Accepted Manuscript*, which has been through the Royal Society of Chemistry peer review process and has been accepted for publication.

Accepted Manuscripts are published online shortly after acceptance, before technical editing, formatting and proof reading. Using this free service, authors can make their results available to the community, in citable form, before we publish the edited article. We will replace this *Accepted Manuscript* with the edited and formatted *Advance Article* as soon as it is available.

You can find more information about *Accepted Manuscripts* in the [Information for Authors](#).

Please note that technical editing may introduce minor changes to the text and/or graphics, which may alter content. The journal's standard [Terms & Conditions](#) and the [Ethical guidelines](#) still apply. In no event shall the Royal Society of Chemistry be held responsible for any errors or omissions in this *Accepted Manuscript* or any consequences arising from the use of any information it contains.

Cite this: DOI: 10.1039/c0xx00000x

www.rsc.org/xxxxxx

Communication

Controlling Interfacial Contact and Exposed Facets for Enhancing Photocatalysis via 2D-2D Heterostructure

Fan Dong^{a*}, Ting Xiong^a, Yanjuan Sun^a, Yuxin Zhang^b, Ying Zhou^c

Received (in XXX, XXX) Xth XXXXXXXXX 20XX, Accepted Xth XXXXXXXXX 20XX

DOI: 10.1039/b000000x

Herein, we report a facile strategy for the creation of 2D layered heterostructure with intimate interfacial contact and exposed reactive facets. The 2D layered heterostructure, intimate contact by sharing the interfacial oxygen atoms and exposed reactive facets endowed the as-prepared BiOIO₃/BiOI nanostructures with highly enhanced visible photocatalytic performance for NO removal.

Recent years have witnessed the boom development of semiconductor photocatalysis with applications in energy conversion, environment remediation and organic synthesis.¹⁻⁵ Heterostructured photocatalysts with enhanced light harvesting and fast charge transfer have attracted particular interest.⁶⁻¹⁰ Beyond zero dimensional (0D) and one dimensional (1D) structures, two dimensional (2D) structure with specific exposed facet, good conductivity or superior electron mobility has received enormous attention.¹¹⁻¹³ Also, 2D-2D heterostructures are more expected than others such as 0D-2D and 1D-2D heterostructures due to the significant advantages of the large contact surface and enhanced charge transfer rate.¹⁴⁻¹⁷ For a desired 2D-2D heterostructure, an intimate and efficient interfacial contact is required to achieve efficient carrier mobility. Photogenerated carriers at the intimate interface are reported to be efficiently transferred and separated.¹⁸ On the other hand, the exposed facet closely related to the photocatalytic performance of heterostructures should be active. Controlling the surface facet exposed to reactants allows us to control the photocatalysis efficiency.¹⁹⁻²⁰ For instance, Zhang et al. reported that BiOCl single-crystalline nanosheets with exposed {010} facets possessed superior activity for indirect dye photosensitization degradation under visible light.²¹ Single-crystal nanosheet based AgSbO₃ with exposed {001} facets prepared by Guo et al. showed enhanced photocatalytic activity for visible-light-driven O₂ evolution.²² Also, TiO₂ with co-exposed {001} and {101} facets forming a surface heterojunction exhibited enhanced photocatalytic performance.²³ Unfortunately, the random synthesis of the 2D layered heterostructures is lack of intimate contact or exposed active facets of the components. Hence, it is highly demanded to develop reliable and controllable strategies for the preparation of 2D layered heterostructures with efficient interfacial contact and active facets.

Bismuth-based semiconductors with layer structure are appealing for multifunctional applications.²⁴⁻²⁹ Among these

materials, BiOI contains a layered structure of alternate [Bi₂O₂] sheets and the I slabs, stacking together by the nonbonding interaction through the I atoms to form a [Bi₂O₂I₂] layer along the c axis as shown in Fig. S1a.³⁰ Most recently, a new Bi-based semiconductor, BiOIO₃, has been found, whose structure can be described as layers of (Bi₂O₂)²⁺ cations structurally analogous to those observed in Aurivillius phase which are connected to (IO₃)⁻ anions (Fig. S1b).³¹⁻³² Such [Bi₂O₂] layered structures tend to guide the lower growth rate along a certain axis to form 2D nanosheets morphology. However, BiOI with high recombination of photogenerated carriers and BiOIO₃ with a wide band gap limit the practical applications of them.

In this work, we integrate the concepts of 2D-2D heterostructure and exposed active facets into one typical nanocomposite of BiOIO₃/BiOI for increased solar absorption and highly enhanced photocatalysis. We tentatively design and construct a unique 2D BiOIO₃/BiOI layered heterostructure. The BiOIO₃ nanosheets with exposed {010} facets are first synthesized. As the atoms arrangement of {010} facets of BiOIO₃ is same with the {001} facets of BiOI, the pristine BiOIO₃ nanosheets then function as substrates to induce the preferential growth of BiOI along (001) plane via providing interfacial oxygen atoms. As the oxygen atoms at the interface are shared by BiOIO₃ and BiOI nanosheets, the large contact areas and intimate interface can be achieved. The detailed procedure for the experiments was described in supporting information (SI). Benefiting from the 2D layered heterostructure with intimate contact by sharing the oxygen atoms at interface, as well as the exposed reactive facets, the as-obtained BiOIO₃/BiOI heterostructures showed promoted visible light photocatalytic efficiency and stability for the removal of ppb-level NO in air. The construction of 2D layer semiconductor heterostructures with intimate contact and exposed facets opens up an unprecedented strategy for the development of highly active visible light photocatalysts for environmental and energetic applications.

The phase and crystal structure of the as-prepared samples were examined by XRD as shown in Fig. 1. The XRD peaks of the BiOIO₃ sample agree well with the orthorhombic BiOIO₃, and the intensified (010) and (040) diffraction peaks compared with the standard card (ICSD # 262019) (Fig. S2) suggest that there is a biased orientations of {010} facets in BiOIO₃. The as-prepared BiOI can be indexed to tetragonal BiOI (JCPDS Card No.73-0062). With an increase in BiOI content in the BiOIO₃/BiOI

heterostructures, the diffraction peaks of BiOI can be observed and the intensity is increased. Notably, the (001) peak of BiOI becomes stronger than the (110) peak in the BiOIO₃/BiOI heterostructures compared with the standard card (Fig. S2) and the as-prepared BiOI. This fact demonstrates that BiOIO₃ could induce the preferential growth of BiOI along the (001) plane.

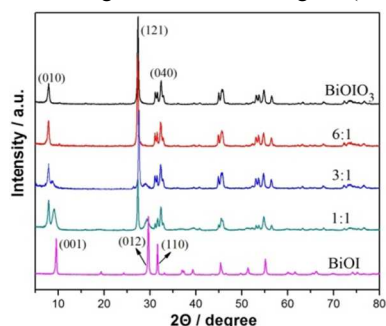


Fig. 1 XRD pattern of the BiOIO₃, BiOI and BiOIO₃/BiOI heterostructures.

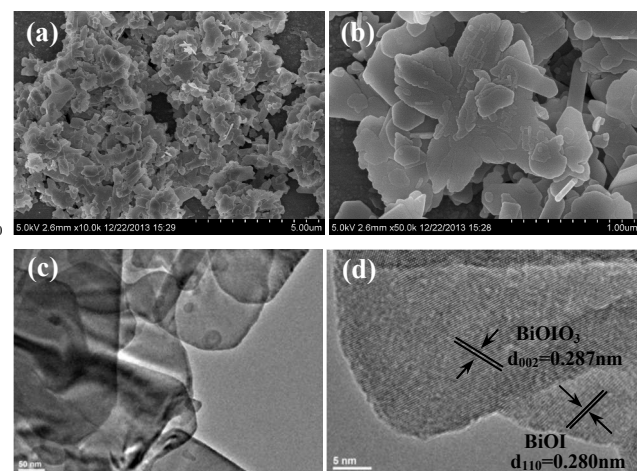


Fig. 2 SEM (a, b) and TEM (c, d) of the as-prepared BiOIO₃/BiOI sample (3:1).

The morphology and microstructure of the samples were characterized by SEM and TEM. For pure BiOI, the obtained samples are nanosheets-shaped structure as displayed in Fig. S3a and S4a. The HRTEM image (Fig. S4b) reveals that the lattice spacing of the nanosheet is 0.30 nm, matching the spacing of the (012) crystal plane of BiOI. The BiOIO₃ with nanosheets feature can be clearly seen in Fig. S3b and S4c. The clear lattice fringe of the interplane is 0.287 nm in the HRTEM image (Fig. S4d), which is in accordance with the (002) crystal plane of BiOIO₃. Combined with the XRD results, it can be found that there is a biased orientations of {010} facets. Thus, we can conclude that the bottom and top surfaces of the BiOIO₃ nanosheets are identified as {010} facets according to the crystal structure.

Fig. 2a shows the low magnification image of the 2D BiOIO₃/BiOI layered heterostructure (3:1) with nanosheets morphology. It can be clearly seen in Fig. 2b and 2c that the samples are constructed by two dimensional layered nanosheets. The lattice fringes with the interplanar spaces of 0.280 and 0.287 nm corresponding to the (110) plane of BiOI and the (002) plane of BiOIO₃ can be observed in Fig. 2d and Fig. S4e, respectively, indicating that the BiOI are grown on the surface of BiOIO₃. This

fact verifies that the construction of 2D BiOIO₃/BiOI layered heterostructures with intimate contact can be readily realized. In addition, based on the strengthened (001) plane revealed by XRD, together with the surface with (110) lattice fringes of the BiOI nanosheets in the heterostructure, we can infer that the BiOI nanosheets in the heterostructure exhibit flat facets of {001} facets. Similar phenomena were observed by Zan et al. who prepared BiOI nanosheets with dominant exposed {001} facets. The BiOI nanosheets with exposed {001} facets showed enhanced photocatalytic activity, and the origin of {001} facets-dependent photoactivity is due to the improved separation efficiency of photo-induced carriers on {001} facets of BiOI.³⁰ Also, the BiOIO₃/BiOI heterostructures with molar ratio of 6:1 and 1:1 present similar layered morphology (Fig. S3c and S3d).

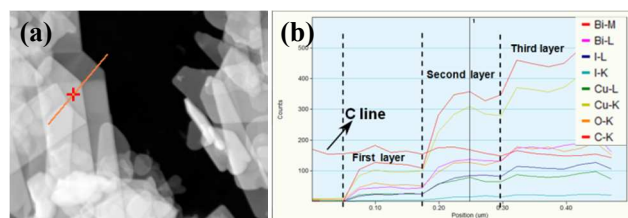


Fig. 3 (b) EDS line scan profiles of Bi, I and O across the samples displayed in (a).

To identify the chemical composition and distribution, we have examined the BiOIO₃/BiOI sample (3:1) by line mapping with energy-dispersive spectroscopy (EDS). The Bi, I and O elemental signals can be clearly observed in selected area in the nanosheet (Fig. 3a). The signals are strengthened gradually (Fig. 3b) along with the red line due to the layer-by-layer assembly. In addition, EDX line spectra and point spectra show the coexistence of Bi, I and O elements (Fig. S5a and 5b), and Cu peaks attributed to the copper foil used as the holder can be observed in EDX analysis.

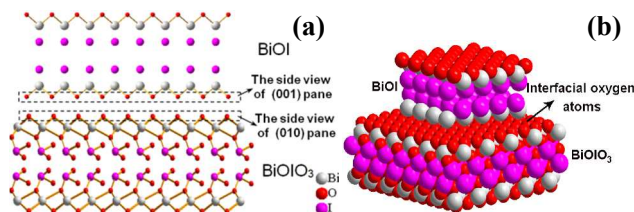


Fig. 4 The side view of the (001) plane of BiOI and the (010) plane of BiOIO₃ (a) and the schematic diagram of BiOI grown on the {010} facets of BiOIO₃ (b).

According to the crystal structures, the atomic structures of the {010} facets of BiOIO₃ and the {001} facets of BiOI are characterized by the high density of exposed oxygen atoms of the (Bi₂O₂)²⁺ layers as illustrated in Fig. 4a. Also, the atoms arrangement of {010} facets of BiOIO₃ is identical to that of the {001} facets of BiOI, which is essential for governing the growth of BiOI along (001) facets. The BiOIO₃ nanosheets with exposed {010} facets are first synthesized. Bi(NO₃)₃·5H₂O dissolved in glacial acetic acid are exist in the form of Bi³⁺ and BiO⁺. As the exposed {010} facets of BiOIO₃ are oxygen atoms, the Bi³⁺ ions in aqueous solution tend to combine with the oxygen of the {010} facets of BiOIO₃. BiOI contains a layered structure of alternate [Bi₂O₂] sheets and the I slabs, stacking together by the nonbonding interaction through the I atoms to form a [Bi₂O₂I₂]

layer along the *c* axis.³⁰ Thus, the latter added I^- ions combine with the Bi atoms via van der Waals force. Then the BiO^+ in aqueous solution interact with the I atoms. Next, the I^- ions interact with the BiO^+ along *c* axis. In this way, BiOI nanosheets are created. Due to the guided growth of the {010} facets of $BiOIO_3$, the BiOI nanosheets are exposed with (001) plane. Consequently, the 2D $BiOIO_3/BiOI$ layered heterostructure with exposed facets are obtained. The oxygen atoms located at the interface are shared by $BiOIO_3$ and BiOI nanosheets, leading to large contact areas and intimate interface (Fig. 4b). Such unique structure could effectively promote the transfer of photogenerated carriers between the two components. N_2 adsorption-desorption isotherms and the BJH desorption pore size distribution plots of the samples are shown in Fig. S6. All the samples have typical Langmuir IV curves with hysteresis loops. The shape of the hysteresis loop is close to type H3 (Fig. S6a), suggesting the existence of slit-like pores formed by aggregation of nanosheet-like particles. The surface area of the $BiOIO_3$, $BiOIO_3/BiOI$ (6:1), $BiOIO_3/BiOI$ (3:1), $BiOIO_3/BiOI$ (1:1) and BiOI was calculated to be 18.3, 11.3, 11.8, 11.4 and 2.9 m^2/g , respectively.

The XPS spectra of the $BiOIO_3$, BiOI and $BiOIO_3/BiOI$ samples (3:1) were further applied to investigate the chemical composition and surface states (Fig. S7). The results (described in SI) further demonstrate the coexistence of $BiOIO_3$ and BiOI. Moreover, compared with the pure $BiOIO_3$ and BiOI, the binding energies of Bi, O and I in $BiOIO_3/BiOI$ heterostructure (3:1) all undergo a chemical shift, indicating the strong interaction between $BiOIO_3$ and BiOI benefiting from the intimate contact. Fig. S8 shows the FT-IR spectra of the five samples. A band corresponding to the vibrations of Bi-O bonds (505 cm^{-1}) can be observed in pure BiOI. For the pure $BiOIO_3$ and heterostructures, except the vibration of Bi-O bonds with two absorption peaks at 404 and 510 cm^{-1} , the intensive peaks at 695 and 764 cm^{-1} attributed to the vibration of I-O bonds can be observed.³³

Fig. S9a displays the samples' optical property investigated by UV-vis DRS. Obviously, $BiOIO_3$ shows an absorption edge around 380 nm, whereas the absorption edge of BiOI is ca. 710 nm. With increasing BiOI amount, the absorption edge of the heterostructures is continuously red-shifted. For a semiconductor, the band gap energy can be calculated by the formula: $\alpha h\nu = A(h\nu - E_g)^n$,³⁴ where α is the absorption coefficient, $h\nu$ is the photon energy, A is a constant and E_g is the band gap. For BiOI and $BiOIO_3$, $n = 4$ for indirect transition. From the $(\alpha h\nu)^{1/2}$ vs. photon energy (Fig. S9b), the band gaps of the BiOI and $BiOIO_3$ (E_g) were estimated to be 1.7 and 3.1 eV, respectively. The valence band-edge potential (E_{VB}) of a semiconductor can be calculated by the empirical equation: $E_{VB} = X - E_c + 0.5E_g$,³⁵ X is the absolute electronegativity of the semiconductor, taken as the weighted average of the X values of the constituents, and E_c is the energy of free electrons on the hydrogen scale (about 4.5 eV). Then, the conduction band bottom (E_{CB}) can be determined by $E_{CB} = E_{VB} - E_g$. For BiOI, the X value is about 5.99 eV, so the E_{VB} is calculated to be 2.34 eV, and then the E_{CB} is estimated to be 0.64 eV. For $BiOIO_3$, the X value is about 7.04 eV, then the E_{VB} is calculated to be 4.09 eV and the E_{CB} is estimated to be 0.99 eV.

To investigate the photogenerated charge separation process, we performed electrochemical impedance spectroscopy (EIS) (Fig. S10). Generally, the smaller arc radius implies a higher

efficiency of charge transfer.³⁶ Obviously, the diameter of the arc radius on the EIS Nyquist plot of $BiOIO_3/BiOI$ (3:1) is smaller than $BiOIO_3$ and BiOI no matter whether it is in the dark or under light irradiation. This fact reveals the enhancement of separation and transfer efficiency of photogenerated electron-hole pairs via the combination of constructing 2D layer heterostructure with intimate interfacial contact and tuning exposed facets.

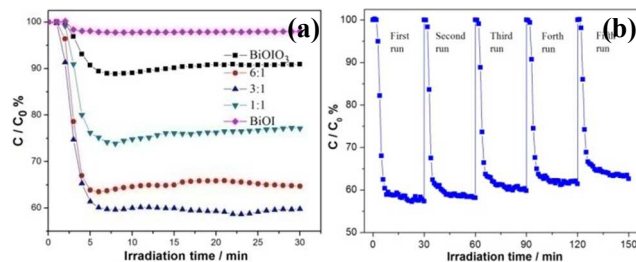


Fig. 5 Visible photocatalytic activities the as-prepared samples (a) and repeated photocatalytic activity of $BiOIO_3/BiOI$ (3:1) (b).

We then tested the photocatalytic performance of the samples by removal of ppb-level NO in air under visible light irradiation ($\lambda > 420\text{ nm}$). Fig. 5a shows that the pristine $BiOIO_3$ nanosheets have a little photocatalytic activity under visible light and the removal ratio is only 9 % in 30 min because of the large band gap. Meanwhile, the BiOI nanosheets show ignorable photocatalytic activity due to the rapid recombination of photoinduced electrons and holes. A small amount of BiOI introduced on the surface of $BiOIO_3$ nanosheets could significantly enhance the NO removal efficiency. The $BiOIO_3/BiOI$ heterostructure (3:1) exhibits the highest photocatalytic activity with a NO removal of 41.3 %, superior to N-doped TiO_2 and g- C_3N_4 .³⁷ Meanwhile, other nanocomposites show slightly lower activity, which is still significantly higher than the pure $BiOIO_3$ or BiOI sample. In addition, the mechanically mixed $BiOIO_3/BiOI$ (3:1) sample with loosely contacted interfaces displays poor photocatalytic activity (Fig. S11). The enhanced photocatalytic activity of $BiOIO_3/BiOI$ samples could be attributed to the heterostructure with intimate contact, 2D layer structure, and the exposed reactive facets.

According to the band energy analyzed by UV-vis DRS part, the potentials of conduction band (CB) of $BiOIO_3$ are more positive than that of BiOI (Fig. 6). Under visible-light irradiation, photogenerated electrons in the CB of BiOI transfer to the CB of $BiOIO_3$ through the intimate interface, while holes are left in the valence band (VB). Such transfer of electrons in the $BiOIO_3/BiOI$ heterostructures could reduce the recombination rate and thus increases the number of carriers to initiate chemical reactions. The potential of the electrons is not negative enough to induce the production of $\cdot O_2^-$. Alternatively, electrons are consumed by multi-electrons reaction to produce H_2O ,³⁸ while holes leaving in the VB of BiOI may directly react with NO or oxidize OH^- to $\cdot OH$ radicals to participate in chemical reaction. Furthermore, the 2D layer structure can also facilitate the transfer of photogenerated carriers and meantime provide more surface active sites. The exposed reactive planes of BiOI not only can improve the separation efficiency of charge carriers, but also can absorb more pollutants, contributing to the photocatalytic reaction. However, excessive BiOI in the heterostructures might reduce the amount of photo-generated charges due to the increased charge recombination by BiOI. Similar phenomena have been observed

for $\text{BiVO}_4/\text{Bi}_2\text{S}_3$ and $\text{Bi}_2\text{MoO}_6/\text{BiOCl}$ photocatalysts.^{7,15} Besides, no apparent decrease in activity can be observed after five consecutive runs (Fig. 5b), suggesting the high stability of $\text{BiOIO}_3/\text{BiOI}$ during the photocatalytic experiments.

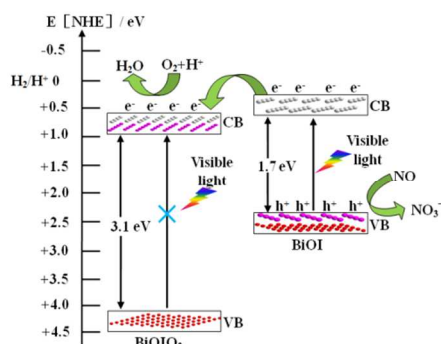


Fig. 6 Schematic diagram of electron-hole pairs separation and the possible reaction mechanism over the $\text{BiOIO}_3/\text{BiOI}$ photocatalysts under visible light irradiation.

In summary, we have developed a facile synthetic approach to construct novel 2D $\text{BiOIO}_3/\text{BiOI}$ layered heterostructures. Since the atoms arrangement of $\{010\}$ facets of BiOIO_3 is the same with the $\{001\}$ facets of BiOI , the pristine BiOIO_3 nanosheets with exposed $\{010\}$ facets induce the preferential growth of BiOI along (001) plane. The shared interfacial oxygen atoms lead to large contact area and intimate contact. The $\text{BiOIO}_3/\text{BiOI}$ heterostructures showed highly enhanced visible photocatalytic activity and stability for NO removal, which was associated with the formation of heterostructure with intimate contact, 2D layer structure and the exposed reactive facets. This work opens up new prospects for constructing other 2D layered heterostructures with intimate contact and exposed active facets. As the 2D structured photocatalysts are abundant, there are numerous opportunities for construction of 2D-2D heterostructures with desired facets. Also, these 2D-2D heterostructures as admirable photocatalysts could find wide applications in environmental remediation and solar-to-fuel energy conversion.

This research is financially supported by the National Natural Science Foundation of China (51478070, 51108487).

Notes and references

^a Chongqing Key Laboratory of Catalysis and Functional Organic Molecules, College of Environmental and Biological Engineering, Chongqing Technology and Business University, Chongqing, 400067, China.

^b College of Materials Science and Engineering, Chongqing University, Chongqing 400044, China.

^c School of Materials Science and Engineering, Southwest Petroleum University, Chengdu, 610500, China.

*To whom correspondence should be addressed.

E-mail: dfctbu@126.com (Fan Dong). Tel./Fax: +86-23-62769785-605.

†Electronic supplementary information (ESI) available: Experimental details, characterization, and Fig. S1 to S11. See DOI: 10.1039/b000000x/

1 Q. J. Xiang, J. G. Yu and M. Jaroniec, *Chem. Soc. Rev.* 2012, **41**, 782.

2 X. C. Wang, S. Blechert and M. Antonietti, *ACS Catal.* 2012, **2**, 1596.

3 S. W. Cao and J. G. Yu, *J. Phys. Chem. Lett.* 2014, **5**, 2101.

4 C. Zhou, Y. Zhao, L. Shang, Y. Cao, L.-Z. Wu, C.-H. Tung and T.

Zhang, *Chem. Commun.*, 2014, **50**, 9554.

5 Y. Wang, X. Wang and M. Antonietti, *Angew. Chem. Int. Ed.* 2011, **50**, 2.

6 H. I. Wang, L. Zhang, Z. Chen, J. Hu, S. Li, Z. Wang, J. Liu and X. Wang, *Chem. Soc. Rev.* 2014, **43**, 5234.

7 X. Gao, H. B. Wu, L. Zheng, Y. Zhong, Y. Hu and X. W. Lou, *Angew. Chem. Int. Ed.* 2014, **53**, 1.

8 F. Dong, Z. W. Zhao, T. Xiong, Z. L. Ni, W. D. Zhang, Y. J. Sun and W. K. Ho, *ACS Appl. Mater. Interfaces* 2013, **5**, 11392.

9 B. Xu, P. He, H. Liu, P. Wang, G. Zhou and X. Wang, *Angew. Chem. Int. Ed.* 2014, **53**, 1.

10 M. Li, Y. Hu, S. Xie, Y. Huang, Y. Tong and X. Lu, *Chem. Commun.*, 2014, **50**, 4341.

11 J. Low, S. Cao, J. Yu and S. Wageh, *Chem. Commun.* 2014, **50**, 10768.

12 J. Yang, D. Voiry, S. J. Ahn, D. Kang, A. Y. Kim, M. Chhowalla and Hyeon S. Shin, *Angew. Chem. Int. Ed.* 2013, **52**, 13751.

13 H. Wang, H. Yuan, S. S. Hong, Y. Li and Y. Cui, *Chem. Soc. Rev.* 2015, DOI: 10.1039/c4cs00287c.

14 J. Zhang, Z. Zhu and X. Feng, *Chem. Eur. J.* 2014, **20**, 1.

15 D. Yue, D. Chen, Z. Wang, H. Ding, R. Zong and Y. Zhu, *Phys. Chem. Chem. Phys.* 2014, **16**, 26314.

16 Y. Li, Y. Liu, J. Wang, E. Uchaker, Q. Zhang, S. Sun, Y. Huang, J. Li and G. Cao, *J. Mater. Chem. A* 2013, **1**, 7949.

17 J. Zhang, Z. Zhu, Y. Tang and X. Feng, *J. Mater. Chem. A* 2013, **1**, 3752.

18 D. Ding, K. Liu, S. He, C. Gao and Y. Yin, *Nano Lett.*, 2014, **14**, 6731.

19 H. G. Yang, C. H. Sun, S. Z. Qiao, J. Zou, G. Liu, S. C. Smith, H. M. Cheng and G. Q. Lu, *Nature* 2008, **453**, 638.

20 G. Liu, H. G. Yang, J. Pan, Y. Q. Yang, G. Q. Lu and H.-M. Cheng, *Chem. Rev.* 2014, **114**, 9559.

21 J. Jiang, K. Zhao, X. Xiao and L. Zhang, *J. Am. Chem. Soc.* 2012, **134**, 4473.

22 J. Shi, J. Ye, Q. Li, Z. Zhou, H. Tong, G. Xi and L. Guo, *Chem. Eur. J.* 2012, **18**, 3157.

23 J. Yu, J. Low, W. Xiao, P. Zhou and M. Jaroniec, *J. Am. Chem. Soc.* 2014, **136**, 8839.

24 R. A. He, S. W. Cao, P. Zhou and J. G. Yu, *Chin. J. Catal.* 2014, **35**, 989.

25 N. Zhang, R. Ciriminna, M. Pagliaro and Y. J. Xu, *Chem. Soc. Rev.* 2014, **43**, 5276-5287.

26 L. Chen, R. Huang, M. Xiong, Q. Yuan, J. He, J. Jia, M.-Y. Yao, S.-L. Luo, C.-T. Au and S.-F. Yin, *Inorg. Chem.* 2013, **52**, 11118.

27 J. Long, S. Wang, H. Chang, B. Zhao, B. Liu, Y. Zhou, W. Wei, X. Wang, L. Huang and W. Huang, *Small* 2014, **10**, 2791.

28 F. Dong, T. Xiong, Y. J. Sun, Z. W. Zhao, Y. Zhou, X. Feng and Z. B. Wu, *Chem. Commun.* 2014, **50**, 10386.

29 F. Dong, Q. Y. Li, Y. J. Sun and W. K. Ho, *ACS Catal.* 2014, **4**, 4341.

30 L. Ye, L. Tian, T. Peng and L. Zan, *J. Mater. Chem.* 2011, **21**, 12479.

31 W. J. Wang, B. B. Huang, X. C. Ma, Z. Y. Wang, X. Y. Qin, X. Y. Zhang, Y. Dai and M.-H. Whangbo, *Chem. Eur. J.* 2013, **19**, 14777.

32 H. W. Huang, Y. He, R. He, X. X. Jiang, Z. S. Lin, Y. H. Zhang and S. C. Wang, *Inorg. Chem. Commun.* 2014, **40**, 215.

33 S. D. Nguyen, J. Yeon, S. H. Kim and P. S. Halasyamani, *J. Am. Chem. Soc.* 2011, **133**, 12422.

34 M. A. Butler, *J. Appl. Phys.* 1977, **48**, 1914.

35 Y. Xu and M. A. A. Schoonen, *Am. Mineral.* 2000, **85**, 543.

36 Z. Hosseini, N. Taghavinia, N. Sharifi, M. Chavoshi and M. Rahman, *J. Phys. Chem. C* 2008, **112**, 18686.

37 (a) F. Dong, Z. Wang, Y. Sun, W.-K. Ho and H. Zhang, *J. Colloid Interf. Sci.* 2013, **401**, 70; (b) F. Dong, S. C. Lee, Z. Wu, Y. Huang, M.

Fu, W.-K. Ho, S. Zou and B. Wang, *J. Hazard. Mater.* 2011, **195**, 346.

38 J. Kim, C. W. Lee and W. Choi, *Environ. Sci. Technol.* 2010, **44**, 6849.